The 10th JFPS International Symposium on Fluid Power FUKUOKA 2017 Oct. 24-27, 2017 The Japan Fluid Power System Society

Research on tribological behavior and lubricating mechanism of slipper pair in axial piston pump under thermal effect

Hesheng Tang*, Yan Ren*, Jiawei Xiang*

* School of Mechanical Engineering, Wenzhou University,
Wenzhou, 325035, China
(E-mail: tanghesheng321200@163.com)

Abstract. The present study is focused on accurate prediction of tribological behavior and lubricating mechanism of slipper pair in axial piston pump under thermal effects. The effects of oil film thickness and stiffness with screening material under thermal conductivity conditions were numerically investigated. In addition, a suitable material combination of the slipper pair was selected though a hydraulic test rig. Based on the theoretical and experimental studies, the combination of QT500-7 and ZY331608 under different surface modification technology was investigated. The results shows that the optimal combination of QT500-7 (nitrogen treatment) and ZY331608 (plasma-sprayed MoS_2) exhibits excellent self-lubricating and anti-wear properties. The lubricating transfer film, such as FeS or Cu_2S, shows the lowest friction coefficient and wear rate. Thus, this combination of screening material is suitable to improve remarkably wear resistance characteristic of slipper pair for axial piston pump under hydrodynamic lubrication condition in comparison with other screening materials.

Keywords: Axial-piston pump, Slipper pair, Lubricating gap, tribological behavior, thermal effect

INTRODUCTION

Axial piston pump is widely used in hydraulic systems because of its advantages, such as high power density, high limit pressure and long service life. There are several challenging issues associated with the pump, such as conflicts between lubrication and wear, and between sealing and leakage. For severe operating conditions, the temperature increase in lubricating region of friction pair may not be ignored. Particularly, slipper and swash plate form key frictional pairs, which will result in significant influences on the performance of pump.

In the earlier researches on the friction pairs of axial piston pump, some simulation models of the oil films were built with programming languages [1]. The most famous independent simulation tool is CASPAR developed by Wieczorek [2]. It was a no isothermal model and took the elastic deformation of friction pairs into consideration. Wang and Yamaguchi [3] theoretically investigated the load carrying capacity, power losses and stiffness of disk-type hydrostatic thrust bearings under eccentric load for elastic and rigid materials respectively. Koc and Hooke [4] had examined the design of hydrostatically balanced bearings used in the slippers of high pressure axial pumps, and outlined a design procedure whereby the slipper behavior, minimum film thickness could be established. In other work, Pang et al. [5] had experimentally investigated the deformation of a slipper bearing under load using photo-elastic measurement techniques. Bergada et al.[6] developed a set of useful analytic solutions for analyzing torque dynamics and barrel dynamics and measured the fluid film thickness, surface erosion and roughness to discuss the effects of oil pressure and temperature. Manring [7] analyzed the behavior of a hydrostatic thrust bearing in a stationary setting. They based their considerations on the fact that during normal operation, the bearing always deforms with either a concave or convex profile being observed. Harris [8] et al. built a dynamic model for slipper pads by bath *fp* simulation package that allows lift and tilt behavior to be predicted and used to examine the dynamic stability of slipper pads over the pumping cycle.

The friction and wear behavior of sliding bearings made from different material combinations under lubrication condition. Several comparison experiments with the bearings designed through the surface coating technology with different components were performed in the past decades. It was reported that solid lubricants (MoS_2)in the form of bonded coatings was an effective way to raise the load carrying capacity of slipper pair under complex lubrication condition. Lovell et al. [9] studied the frictional behavior of the MoS_2-coated ball bearings. The chemical and the physical features present in coated thrust bearings are further investigated using scanning electron microscopy and chemical spectroscopy techniques. Wahl and Singer [10] studied the effect of different mass transfer flows in the performance of MoS_2 coatings by the sliding tests. For better understanding of the wear mechanism in slipper pair, it is necessary to observe the tribological behavior of screening material using standard pin-on-disk sliding test with tribometers.

This research will focus on tribological behavior and lubricating mechanism of slipper pair for axial piston pump. The outline of the current paper is as follows: (a) the oil lubricating mechanism of slipper pair under thermal effects will be investigated; (b) tribological performance of matching materials between the slipper and swash plate will be experimentally is studied, considering the effects of various material combinations and surface treatment method, and then the suitable material combinations of the slipper pair will be screened out.

ESTABLISHMENT OF MATHEMATICAL MODEL

2.2. Film thickness model

The external forces applied on the slipper pair is shown in Fig. 2. The inertial force of the piston bore caused by non-constant flow is not considered. The hydraulic clamping force caused by the piston structure. Axial hydraulic dynamics force in the oil film for slipper pair is mainly affected by the external force, including hydraulic force, the return spring force, the axial inertial force, the friction force caused by centrifugal force and cylinder bore friction reaction forces.

With the coordinate system of Figure 1, the force balance equation on the *z*-axis of slipper pair is listed.

$$F_z\cos\beta - f\left(F_1+F_2\right) - F_p - F_r - F_f - F_a = 0 \qquad (1)$$

where F_z is *z*-axial force, F_p is hydraulic force, F_r is return spring force, F_f is friction force caused by centrifugal force, F_a is axial inertial force, β is swash plate angle. F_1, F_2 is acting forces of piston, f is friction coefficient.

Therefore, the axial force acting on the slipper can be obtained

$$F_z = \frac{f\left(F_1+F_2\right)+F_p+F_r+F_f+F_a}{\cos\beta} \qquad (2)$$

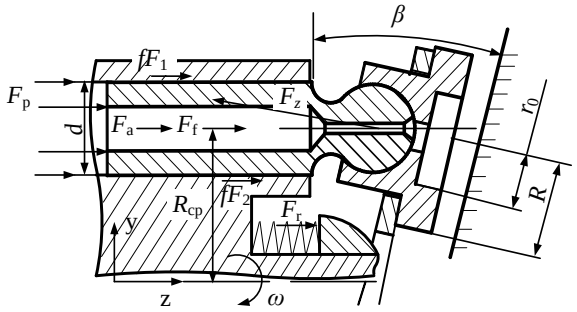

Figure 2. External forces applied on the slipper.

In addition, the bearing force from oil film includes hydraulic force, thermal wedge bearing force and squeezing force. The thermal wedge bearing force is written as [11]

$$F_t = \frac{\alpha_p\mu^2\omega_s^2}{Gc_p\rho g\delta^4}\left[6R^2\left(1+\tan^2\beta\cos^2\omega t\right)\left(R^2-r_0^2\right)+\left(R^2-r_0^2\right)\right] \qquad (8)$$

where R is slipper outside radius, r_0 is slipper inside radius, α_p is pressure coefficient, μ is oil viscosity, G is equivalent power, ω_s is angular velocity of slipper, ρ is oil density, c_p is fluid specific heat, g is acceleration of gravity, δ is film thickness, t is simulation time.

The squeezing force equation at sealing land of slipper can be described as [11].

$$F_s = \int_{r_0}^{R} 2\pi rpdr = \frac{3\pi\mu}{2\delta^3}\left(-\frac{\mathrm{d}\delta}{\mathrm{d}t}\right)\left[\left(R^4-r_0^4\right)-\frac{R^2-r_0^2}{\ln\left(R/r_0\right)}\right] \qquad (9)$$

where F_s is squeezing force, p is film pressure, r is slipper radius.

The hydrodynamic bearing force is written as [11].

$$F_h = \frac{3\mu vLRr_0\left(R-r_0\right)l_1}{r_0\delta^3+\left(R-r_0\right)\left(l_1+\delta\right)^3} \qquad (10)$$

where F_h is hydrodynamic bearing force, v is slipper velocity, L is width of slipper sealing land, l_1 is depth of groove.

Thus, submitting Eqs. (6)- (10) into Eq. (11), the slipper pocket pressure can be expressed as

$$p_s = \frac{2\ln(R/r_0)}{\pi(R^2 - r_0^2)}(F_z - F_t - F_s - F_h) \quad (11)$$

According to the principle of fluid continuity, the ratio of fluid pressure in slipper pocket can be written as

$$\frac{p_s}{p_p} = \frac{1}{1 + \frac{64l}{3d_s{}^4 \ln(R/r_0)}\delta^3} \quad (12)$$

Substituting Eq. (12) into Eq. (11), the film thickness can be calculated by

$$F_z - F_t - F_s - F_h - \frac{\pi(R^2 - r_0^2)}{2\ln(R/r_0)} \frac{p_p}{1 + \frac{64l}{3d_s^4 \ln(R/r_0)}\delta^3} = 0 \quad (13)$$

Since the thermal wedge bearing force (F_t), squeezing force (F_s) and hydrodynamic bearing force (F_h) are obtained, the value can be submits into Eq. (13), in which the film thickness is investigated.

2.3 Temperature-dependent viscosity model

The control volume of fluid film within slipper pair is subjected to two major heat sources: the heat coming from the viscous dissipation associated with the fluid flow in the lubricating interfaces and in the heat generated due to the rotation of the slipper and swash plate in the oil-filled case. Thus, the overall oil film temperature on the slipper pair can be calculated by

$$\frac{dT}{dt} = \frac{1}{c_p m}\left[p_s \frac{dV}{dt} + \sum \dot{m}_{in}(H_{in} - H) + \sum \dot{m}_{out}(H_{out} - H) + m a_p T \upsilon \frac{dp_s}{dt} \right] \quad (14)$$

In addition, viscosity is one of the important factors that affect the oil drive characteristics. Temperature has considerable influence on the oil viscosity. At present, ISO VG12 aviation hydraulic oil is usually used as the working medium for the pump, whose density is 900 kg/m^3, and the dynamic viscosity is 0.018 Pa s at 40 ℃. Since the experimental data are discrete temperature points, the temperature-dependent viscosity is written as

$$\mu = 2.961\times10^{-5}(T-273)^2 - 1.827\times10^{-2}(T-273)^2 + 2.835 \quad (15)$$

Therefore, substituting Eq. (15) into Eqs. (8)-(9), the thermal wedge bearing force and thermal wedge bearing force are investigated.

2.4 Heat transfer model

In this section, the heat transfer process between oil film and slipper pair in axial piston pump is described. In order to select the appropriate heat transfer correlation during operation, the heat transfer regime of slipper pair is specified. When fluid flows from piston chamber into slipper central chamber, the convective heat exchange between the fluid film and slipper is written as [11]

$$\dot{Q}_1 = \frac{T - T_c}{\frac{1}{h_{as} 2\pi r_0 H_1} + \frac{\ln(R/r_0)}{k_1 2\pi H_1} + \frac{1}{h_{asp} 2\pi R H_2}} \quad (16)$$

where $\dot{Q}_1$ is heat transfer rate of slipper, T_c is case temperature, H_1 is slipper's lug height, H_2 is swash plate height, k_1 is slipper thermal conductivity, h_{as} is convective heat transfer coefficient of slipper, h_{asp} is convective heat transfer coefficient of swash plate.

The convective heat exchange between the fluid film and swash plate is written as [11]

$$\dot{Q}_2 = \frac{T - T_c}{\frac{1}{h_{asp}\pi R^2} + \frac{H_2}{k_2 \pi R^2} + \frac{1}{h_{asp}\pi R^2}} \quad (17)$$

where $\dot{Q}_2$ is heat transfer rate of swash plate, k_2 is swash plate thermal conductivity.

The convective heat exchange between leakage fluid and case fluid is calculated by follows

$$\dot{Q}_3 = \lambda 2\pi R \delta (T - T_c) \quad (18)$$

where $\dot{Q}_3$ is heat transfer rate of fluid, λ is fluid heat conduction coefficient.

Therefore, the total heat generation within control volume of fluid film through heat transfer mode can be written as

$$\dot{Q} = \dot{Q}_1 + \dot{Q}_2 + \dot{Q}_3 \tag{19}$$

where $\dot{Q}$ is total heat transfer rate of fluid film.

Since the total heat generation within control volume of fluid film is obtained, the value can be submits into Eq. (14), in which the oil film temperature is investigated.

2.5 Load carrying model

The support force that acts to resist the external load applied in slipper, denotes the load-carrying capacity of slipper pair. Thus, the load carrying capacity of slipper pair can be written as follows

$$J = \frac{\mathrm{d}\left(\frac{p_s}{p_p}\right)}{\mathrm{d}\delta} = \frac{32\pi l}{d_s^4} \cdot \frac{\left(R^2 - r_0^2\right)}{\left[\ln\left(R/r_0\right)\right]^2} \cdot \frac{p_s \delta^2}{\left[1 + \frac{64l}{3\ln\left(R/r_0\right) d_s^4}\delta^3\right]^2} \tag{20}$$

THEORETICAL RESULT

3.1 Effect of oil temperature

Fig. 10 illustrates effect of temperature on average film thickness. During the delivery stroke, the average film thickness is lower than that during the suction stroke. As the oil temperature increases from 50 ℃ to 90 ℃, there is a prominent decrease in the average thickness of the lubricating oil film during the suction stroke. Especially when the oil temperature is 90 ℃, the oscillation amplitude of average film thickness becomes smaller in the transition region, which in turn implies the breaking of the oil film. Two factors contribute to this influence, the squeezing force and thermal wedge bearing force acting on the slipper. The squeezing force increases dramatically as the oil temperature increases from 50 ℃ to 90 ℃. At the same time, the thermal wedge bearing force becomes larger, which leads to increase viscous heat generation at the film gap between slipper and swash plate. These factors result in generating high clamping force acting on slipper that causes film thickness decrease. For high oil temperature condition, the slipper is unable to find equilibrium due to the larger thermal wedge bearing force, and the variation of oil film thickness is not compromised while the slipper is strongly unstable.

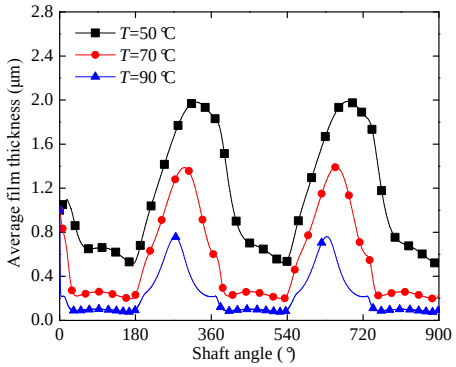

Fig. 10 Effect of temperature on average film thickness

Figure 11 shows effect of temperature on load carrying capacity of slipper pair. The load carrying capacity of slipper pair periodically changes with shaft angle and increases as the film temperature increases. The physics phenomenon is related to the film stiffness that is defined as the gradient of load carrying capacity. This film stiffness changes with different film temperature. As the film thickness decreases, the load carrying capacity for high oil temperature increases faster than the low oil temperature, implying that the film stiffness increases as the temperature increases. There are two factors that affect the load carrying capacity. They are the film thickness and the oil viscosity. During delivery strokes, the load-carrying capacity increases with a high decline in the film thickness, while decreasing the fluid viscosity increases the load carrying capacity. As the film thickness drops, the temperature increases rapidly, the viscosity of the oil drops, and the overall result is a rather high increase in the load-carrying capacity.

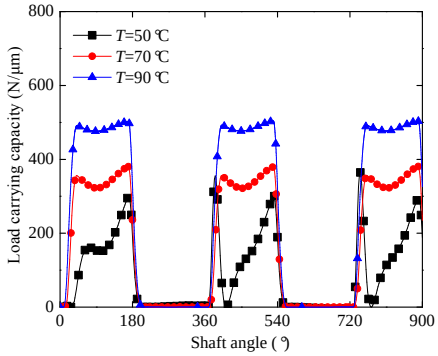

Fig. 11 Effect of temperature on load-carrying capacity of slipper pair

3.2 Parameter influence

Fig.16 shows the effect of slipper radius ratio on average film thickness and load carrying capacity. It can be seen that the film thickness decreases rapidly with increasing slipper radius ratio, but the load-carrying capacity becomes larger. This is because as the slipper radius ratio increases, there is less hydrodynamic bearing force on the sealing land area of slipper but larger squeezing bearing force, resulting in film thickness reduction. With increase of squeezing bearing force, the average film thickness becomes thinner and result in breaking of lubricating oil film and abrasion wear of slipper. Thus, although the load carrying capacity of slipper pair increases, there is no benefit of making slipper radius ratio larger than that corresponding to the minimum value of average film thickness. To take advantage of hydrodynamic bearing force and squeezing bearing force, the slipper radius ratio should be selected from1.4 to 1.8.

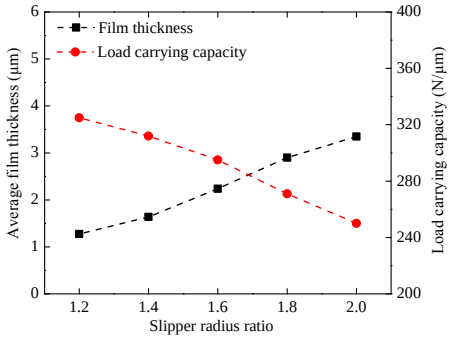

Fig. 16 Effect of slipper radius ratio on average film thickness and load carrying capacity

Fig. 17 shows the effect of the orifice length diameter ratio on average film thickness and load carrying capacity. In Fig. 17, it can be found that average film thickness drops as the orifice length diameter ratio increases, but the load carrying capacity increase. Two factors contribute to this influence, the squeezing bearing force and the pressure drop along the orifice. As orifice length diameter ratio increases, the pressure drop along the orifice increase, which leads to high squeezing force generation, and result in the film pressure buildup reduction. Thus, the orifice length diameter ratio is very important in determining the load carrying capacity of slipper pair. For low orifice length diameter ratio, the average film thickness increase, but at the same time, the load carrying capacity will also decrease. For high orifice length diameter ratio, average film thickness becomes thinner, but the load carrying capacity will increase sharply. Considering all the above issues, it may be recommended that the orifice length diameter ratio should be selected from 4 to 5.

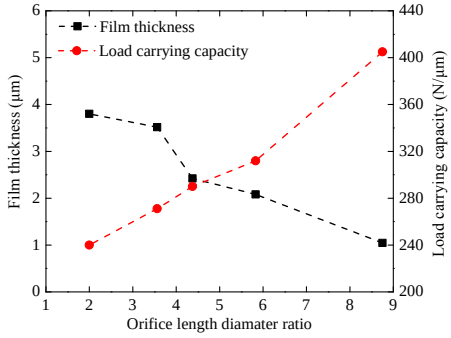

Fig. 17 Effect of orifice length diameter ratio on average film thickness and load carrying capacity

EXPERIMENT RESULT

Friction and wear tests were conducted on a MMS2A ring-on block test rig, as shown in Fig. 1. The tester connected to a computer was used to evaluate the friction coefficient and temperature of the friction pairs under oil lubrication. Fig. 2 shows the installation drawing of the friction pairs. The dimensions of upper specimen block was 6 mm (length) × 7 mm (width) × 3 mm (height). The dimensions of bottom specimen ring was Ø 16 mm (outer diameter)× Ø 40 mm (inner diameter) ×3 mm (height). The experiments were performed with rotational speed of 400 r/min, load of 400 N, and a period of 2 h. The test rig was powered in room temperature. Before the experiment, the water box was filled with enough seawater to immerse completely the upper and bottom specimens in lubricant oil. Friction coefficients and wear capacities are calculated by theoretical formulae, respectively. After the friction test, the worn morphologies of the specimens were observed under a laser scanning microscope.

Fig. 1 Wear measurement apparatus of type MMS2A and specimen

4. 1 Friction Coefficient and Wear Rate

Fig. 1 shows the variation of the friction coefficient of two kinds of friction pairs with test time. At start stage (0~1200s), the surface roughness of pairing material is relatively high and the contact area is small so that the friction coefficient fluctuated around 0.125-0.135 and the amplitude of fluctuation is small. At the stable stage (1200-4800s), due to the transfer lubricating film formed on the friction surface of pairing material, the friction coefficient of A1 and A2 were fluctuated at about 0.135 and 0.125, respectively. During the stable stage, the friction coefficient is related to certain factors, such as the properties of material, load and sliding speed. At the intense stage (4800~7200s), the transfer lubricating film on the surface of pairing material ruptures, which directly contact the friction surface between upper and bottom specimens and cause oil temperature rise. In this stage, the friction coefficient of material change with the variation of oil temperature. Compared with the friction coefficient of A1 and A2, the friction coefficient of A1 was much higher than that of A2. The friction coefficient of A2 is 0.12~ 0.13, and the variation of friction coefficient is small. The sulfur atom in the MoS_2 coating has a higher activity on copper element and iron element so that the surface of the dual material forms transfer lubricating film under the action of friction and heat stress. The transfer lubricating film is composed of Cu_2S and FeS, which improves wear resistance of pairing materials and reduces friction coefficient.

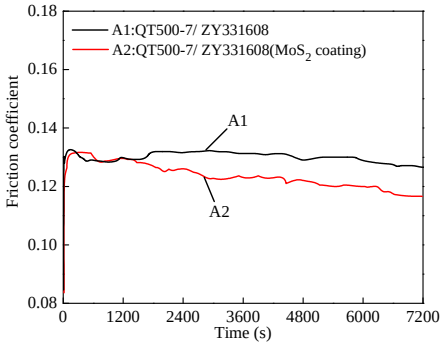

Fig.1 Friction coefficient of pairing material surface under different surface treatments

Fig. 4 shows wear rate of pairing materials under different surface treatments. Under the same load, the wear rate of the dual material in the group of A2 is the smallest. In the group of A2, the wear rate of QT500-7 and ZY331608 were stable at about 2.17×10^{-9} $mm^3/N\cdot m$ and 7.63×10^{-8} $mm^3/N\cdot m$, respectively. This result can be explained that the heat was accumulated on the friction surface of material due to sliding against each other, which lead to increase the contact surface temperature of friction pair. The shear strength of material decreases with the increasing surface temperature. In this condition, the micro-convexes on the surface of friction pair is easier to wear, and increase the wear rate of pairing materials. In friction process, the surface of ZY331608 after plasma spraying MoS_2 treatment is easy to form transfer lubricating film with Cu_2S, which improve the hardness

and shear strength of materials. The heat dissipation condition between QT500-7 and ZY331608 is improved. In addition, MoS_2 coating has strong adsorption capacity, and it has high bonding strength with metal material. Therefore, the ZY331608 with MoS_2 coating has better antifriction and anti-wear properties which is useful to decrease wear rate of material.

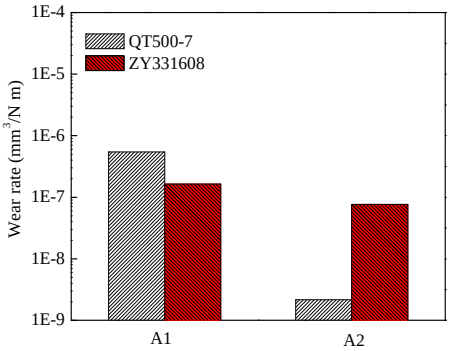

Fig.4 Wear rate of pairing materials under different surface treatments

4.2 Worn Surface of Specimens

Fig.6 shows the worn morphologies of QT500-7 (nitriding treatment) and ZY331608 before and after the tests. As shown in Fig.6a, the white part of the surface morphology of QT500-7 after nitriding treatment is bright white layer of nitrided surface, which is composed of particle distribution. The hardness of nitrided layer is the biggest, and the wear resistance is the strongest. The black part of nitrided surface is the diffusion layer, which is relatively loose. The hardness of the material decreases with the increase of wear depth. When the wear depth of the material reaches the penetration layer and matrix of QT500-7, the wear resistance of the material decreases sharply. In Fig.6b, a large number of spalling pits are formed on the friction surface of QT500-7. This result can be explained that the white layer with high surface hardness and the diffusion layer in the middle part of QT500-7 due to large shear stress are separated quickly in the friction process. Compared with Fig. 6c and Fig. 6d, the contact surface of ZY331608 has worn obvious furrow, and the direction of furrow parallels to the sliding direction. There are some debris in the furrow around. This phenomenon can be explained that the soft substrate of material in the local extrusion will form to small hard particles. In addition, the external force on the specimen surface can be divided into normal force and tangential force. On the one hand, the hard particles are pressed into the surface of the specimen under the normal force; On the other hand, the sample surface was cut in to furrow shape of wear trace by hard particles due to action of tangential force.

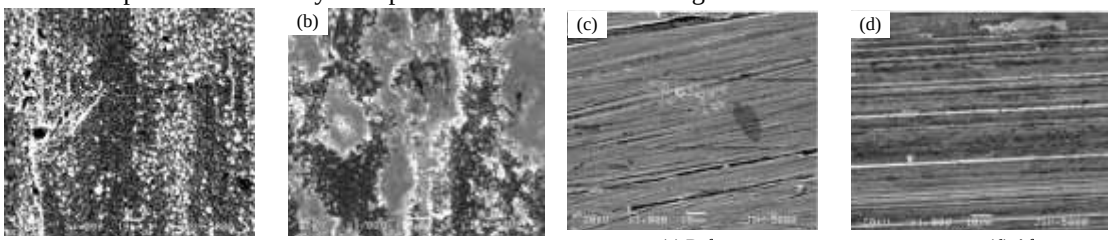

Fig.6 Electron microscopy observations of QT500-7 (Nitriding treatment) and ZY331608

Fig.7 shows the worn morphologies of QT500-7 (nitriding treatment) and ZY331608 (plasma spraying MoS_2 treatment) before and after the tests. Compared with Fig. 7a and Fig. 7b, a large spalling pit are formed along the frictional sliding direction on the friction surface of QT500-7. In the Fig.7b, the number of spalling pits is decreased, and the depth of pit is shallow. Compared with 7C and 7d, it can be seen that the worn surface of ZY331608 is smooth. There are no obvious wear trace after the test, but the convex crystal particle are worn. The shedding phenomenon of worn face is not obvious. The adhesion wear and abrasive wear of materials are significantly reduced. The result can be explained that the MoS_2 coating can obviously improve the friction and wear resistance of the multi-element complex brass, which can be explained by the crystal structure particularity of MoS_2. The MoS_2 has the characteristics of six layered lattice with compact arrangement, which the deformation resistance of material is so small that slips easily along the surface. The copper element in the contact surface react with sulfur atoms to form the transfer lubricating film composed of Cu_2S, which plays a role in reducing friction and lubrication on the friction materials.

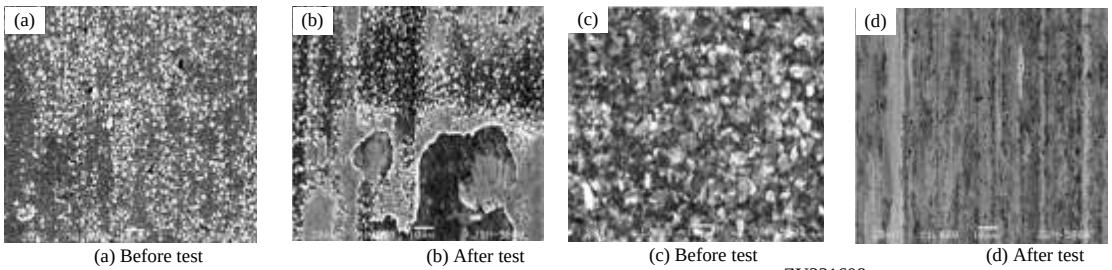

Fig.7 Worn morphologies of QT500-7 (Nitriding treatment) and ZY331608(Plasma-spraying MoS_2)

CONCLUSIONS

(1) As oil temperature increases, the film thickness decreases, but the load-carrying capacity will increase dramatically. The squeezing force and thermal wedge bearing force are main factors that affect film thickness and load carrying capacity. At high oil temperature, there is high viscous dispassion at the film gap, which leads to increase thermal wedge bearing force. Because the combination action of squeezing force and the thermal wedge bearing force become larger, the film thickness decreases with increasing clamping force, but load-carrying capacity of slipper pair will increase.
(2) Slipper radius ratio and orifice length diameter ratio have significant influence on the film thickness and load carrying capacity behaviors. If the slipper radius ratio increases, the film thickness decreases, but the load carrying capacity will increase sharply. As the slipper radius ratio increases, there is larger squeezing bearing force on the sealing land area of slipper, resulting in thinner film thickness.
(3) In friction process, the surface of ZY331608 after plasma spraying MoS_2 treatment is easy to form transfer lubricating film with Cu_2S, which improve the hardness and shear strength of materials.

ACKNOWLEDGMENTS

This paper is supported by the Notional Natural Science Foundation of China (No.51505338) and the Youths Science Foundation of Zhejiang (No. LQ16E050004 and No. LQ17E050003).

REFERENCES

1. MANDERS, N. D., Friction Forces within the Cylinder Bores of Swash-plate Type Axial-piston Pumps and Motors, J.Dyn.Sys.,Meas., Control, 1999, 121(2), pp.531-537.
2. WIECZOREK U, IVANTYSYNOVA M. Computer Aided Optimization of Bearing and Sealing Gaps in Hydrostatic Machines - the Simulation Tool CASPAR. International Journal of Fluid Power, 2002, 3(1), pp.7-20.
3. WANG, X., YAMAGUCHI, A. Characteristics of Hydrostatic Bearing/Seal Parts for Water Hydraulic Pumps and Motors. Part 1: Experiment and Theory, Tribology international, 2002, 35(1), pp.425-433.
4. KOC, E., HOOKE C.J., Investigation into the Effects of Orifice Size, Offset and Overclamp Ratio on the Lubrication of Slipper Bearings. Tribology international, 1996, 29(4), pp. 299-305.
5. PANG, Z., ZHAI, W., SHUN, J. The Study of Hydrostatic Lubrication of the Slipper in a High-Pressure in a High-Pressure Plunger Pump. STLE Tribol. Trans.1993, 36(2), pp.316-320.
6. BERGADA, J.M, DAVIES, D.L, KUMAR, S, WATTON, J. The Effect of Oil Pressure and Temperature on Barrel Film Thickness and Barrel Dynamics of An Axial Piston Pump. Meccanica., 2012, 47(3), pp.439-654.
7. MANRING N.D, WRAY C.L, ZHILIN Dong. Experimental Studies on the Performance of Slipper Bearings within Axial-Piston Pumps. Journal of Tribology, 2004, 126(4), pp.511-522.
8. HARRIS, R.M, EDGE, K.A, TILLEY,BD.G. The Suction Dynamics of Positive Displacement Axial Piston Pumps. J.Dyn.Sys.,Meas.,Control, 1994,116(2), pp.1-7.
9. LOVELL, M.R., KHONSARI, M.M, MARANGONI, R.D., Frictional Analysis of MoS_2 Coated Ball Bearings: A Three-Dimensional Finite Element Analysis, Journal of tribology, 1997; 119(4), pp.754-763.
10. WAHL, K.J., BELIN, M., SINGER, I.L., A Triboscopic Investigation of the Wear and Friction of MoS_2 in a Reciprocating Sliding Contact. Wear. 1998, 214(2), pp.212-220.
11. WEN, D.S., Innovation and development of hydraulic components [M]. Beijing: Aviation Industry Press, 2009 [Chinese].

